Spatially and Spectrally Resolved Narrowband Optical Absorber Based on 2D Grating Nanostructures on Metallic Films

Yurui Qu, Qiang Li,* Hanmo Gong, Kaikai Du, Songang Bai, Ding Zhao, Hui Ye, and Min Qiu

Two spatially and spectrally resolved narrowband absorbers based on 2D grating nanostructures (polymethylmethacrylate (PMMA) grating and gold grating) on metallic films are designed, fabricated, and characterized. For PMMA grating on a metallic film, the measured absorption bandwidth is 12 nm with a nearly 80% absorption at normal incidence. The transverse electric (TE) localized mode shows a calculated 3.5° angular width. The transverse magnetic (TM) resonant mode supports both a localized mode and a lattice mode. The TM lattice mode shows a calculated angular width of 0.75° and exhibits a large wavelength-angle sensitivity of nearly 15 nm per degree and a large absorption-angle sensitivity of 77.5% per degree. For gold grating on a metallic film, the measured absorption bandwidth is 40 nm with a nearly 70% absorption. Such spatially and spectrally resolved 2D nanostructure arrays with large angle sensitivities have potential applications in angle measurement, thermal emitters, optical filters, and biosensors.

1. Introduction

High-performance optical absorbers have garnered great interest because of their wide applications in solar thermophotovoltaic systems, sensors, photodetectors, photo-thermal modulators, etc.[1–4] Take the high resolution angle measurement in spatial optical sensing as an example, the widely used techniques are mainly based on autocollimators,[5,6] interferometers,[7,8] and total internal reflection,[9,10] which involve complex optical system and optical elements such as beam splitter, right angle prism, and mirror. By applying optical absorbers in spatial optical sensing, the size as well as the weight can be significantly reduced. Besides, the spatially resolved absorber can be used as a filter for spatial signal processing.[11]

So far, a lot of strategies have been demonstrated to realize high optical absorption, including metal–insulator–metal plasmonic absorbers based on magnetic resonances,[12–24] highly absorbing dielectric on metal exploiting strong interference

effects,[25,26] film stacks-based Fabry–Pérot (FP) cavity absorber,[27,28] shallow grating,[29–32] metallic convex groove plasmonic absorber with adiabatic nanofocusing,[33,34] metallic surfaces with grooves,[35,36] etc. For spatial optical sensing and signal processing, the spatially and spectrally resolved narrowband absorbers (whose absorption strongly depends on the incident angle) are highly desirable. Of all the aforementioned absorbers, film stacks-based FP cavity absorber demonstrates a good spatially and spectrally resolved narrowband characteristic; however, its cavity length is limited to quarter-wavelength since it is dependent on multipass transmission phase shifts. The metallic shallow grating-based optical absorber, which utilizes surface plasmon polaritons (SPPs) at metal–dielectric interface,[37,38] shows the ability of confining light beyond the diffraction limit and thereby significantly reduces the device thickness. This absorber has shown spatially and spectrally narrow-band absorption with a 1D metallic shallow grating configuration[29,39] or a 2D ring-based grating configuration[30] at normal incidence. However, its spatially-resolved characteristic is still to be explored. Considering its potential applications in spatial optical measurement and signal processing, it is of vital importance to study its spatially-resolved characteristic.

In this paper, two kinds of spatially and spectrally resolved narrowband absorber based on 2D grating nanostructures on metallic films are presented: a PMMA nanohole array and an Au nanodisk array on metallic films. Both spatially and spectrally resolved narrowband absorption under both TE and TM polarizations is experimentally demonstrated. For the TE polarization, the absorption corresponds to a localized mode. For the TM polarization, both a localized mode and a lattice mode can be obtained. For angle measurement utilizing the TM lattice mode, it could show a large measurement range (between −30° and 30°) and a relatively low resolution (10^{-3} degree) by resolving the peak resonant wavelength. A small measurement range (within 0.75°) and an extremely high resolution (10^{-7} degree) can also be obtained by resolving the resonant absorbance. Therefore, these spatially and spectrally resolved narrowband absorbers have a potential application for spatial optical measurement and signal processing.

Dr. Y. Qu, Prof. Q. Li, Dr. H. Gong, Dr. K. Du,
Dr. S. Bai, Dr. D. Zhao, Prof. H. Ye, Prof. M. Qiu
State Key Laboratory of Modern Optical Instrumentation
College of Optical Science and Engineering
Zhejiang University
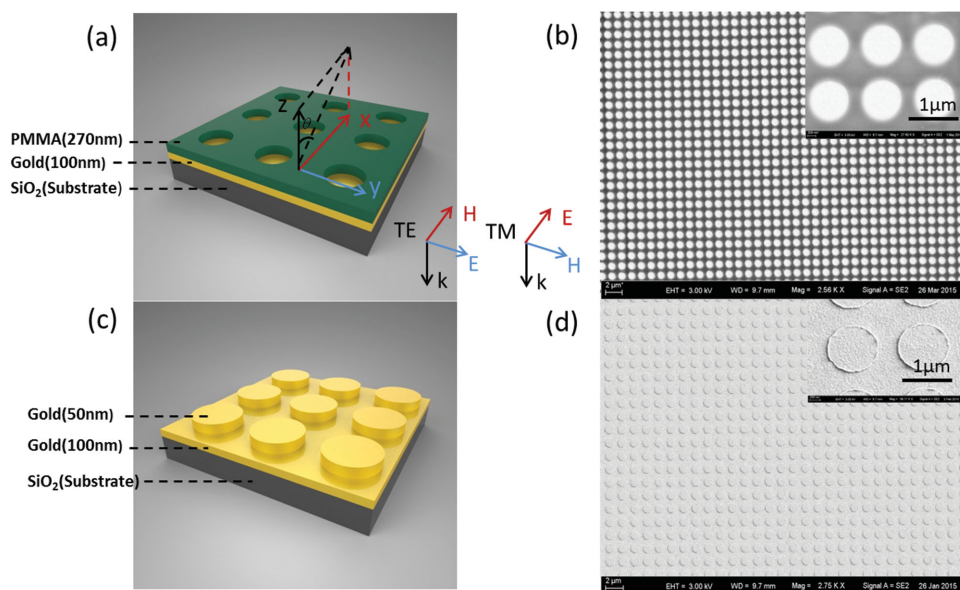310027 Hangzhou, China
E-mail: qiangli@zju.edu.cn

Figure 1. a) A schematic and b) an SEM image of a PMMA 2D periodical nanohole array absorber. c) A schematic and d) an SEM image of an Au 2D periodical nanodisk array absorber. TE and TM incidences are denoted. θ represents the incident angle in the incident x–z plane.

2. Results and Discussion

The two kinds of spatially and spectrally resolved narrowband absorber are provided in **Figure 1**. The first kind is composed of a 2D periodic nanohole array in PMMA on an Au film (termed as "PMMA absorber"), as shown in Figure 1a. The second kind consists of a 2D periodic Au nanodisk array on an Au film (termed as "Au absorber"), as depicted in Figure 1c. Figure 1b,d presents corresponding scanning electron microscope (SEM) images. The periodic nanostructures are fabricated on top of thick enough (100 nm) gold films in order to prevent light transmission. For the PMMA absorber, the nanohole thickness, the nanohole radius, and the array periodicity are 270, 440, and 1400 nm, respectively. For the Au absorber, the nanodisk thickness, the nanodisk radius, and the array periodicity are 50, 500, and 1400 nm, respectively. The total dimensions of the nanostructure arrays are 300×300 μm^2. The fabrication of these two absorbers is described in the Experimental Section and the Supporting Information.

The spatially and spectrally resolved absorption (A) is measured using a home-made reflection measurement setup (see Supporting Information Figure S2). The light beam from a super-continuum light source is focused through a lens with a focal length of 45 mm. The light could be confined to about 50 μm in diameter when reaching the sample. For the reflection, another identical lens is exploited to couple the light into an optical spectrum analyzer. Since the transmission can be neglected considering the 100 nm Au film, the absorption (A) can be obtained by $A = 1 - R$, with R being the reflection. The spatially and spectrally resolved absorption is measured at both polarizations (TE and TM). For TE and TM modes, the electric field and magnetic field are perpendicular to the xz incident plane (S_{xz}), respectively, as shown in Figure 1.

Figure 2a,b shows the measured spatially and spectrally resolved absorption of the PMMA absorber. At normal incidence (there is no difference between TE and TM modes in this scenario), the absorption peak "locates" at 1350 nm. The full width at half maximum of absorption band is as narrow as 12 nm and the maximum absorption is close to 80%. At oblique incidence, the absorption peaks of both TE and TM modes are sensitive to the incident angle. For the TE mode, the absorption peak exhibits a blueshift with an increasing incident angle. Specifically, the absorption peak shifts from 1357 to 1332 nm when the incident angle increases from 0° to 15°. To characterize the spatial resolving ability of this absorber in terms of the resonant wavelength, here we define the wavelength-angle sensitivity (dλ/dθ) (peak wavelength shift $\Delta\lambda$ divided by the incident angle variation $\Delta\theta$ with a unit of nm per degree). The measured wavelength-angle sensitivity of TE mode is almost 1.7 nm per degree. For the TM mode, two strong absorption peaks can be observed. As the incident angle increases, one absorption peak shows a large redshift and another shows a large blueshift. Specifically, the two absorption peaks are shifted to 1205 and 1505 nm at 10° incident angle, which corresponds to a large wavelength-angle sensitivity of nearly 15 nm per degree. A weak absorption peak, which is not as sensitive to the incident angle as two strong peaks, can also be observed. This absorption mode exhibits a small wavelength-angle sensitivity of only 2.1 nm per degree.

The spatially and spectrally resolved absorption is also calculated using commercial software COMSOL MULTIPHYSICS. The refractive index of PMMA is taken to be 1.75. The relative permittivity of Au is modeled using the Drude model,[40] i.e., $\varepsilon(\omega) = \varepsilon_\infty - \omega_p^2/(\omega^2 - i\omega\,\Gamma)$, with $\varepsilon_\infty = 9.0$, $\omega_p = 1.3673 \times 10^{16}$ s^{-1}, and $\Gamma = 1.0027 \times 10^{14}$ s^{-1}. The Drude model provides excellent agreement with the measured optical constants of Johnson and Christy data in the spectral range of interest. Figure 2c,d provides the calculated spatially and spectrally resolved absorption of the PMMA absorber, agreeing with experimental results.
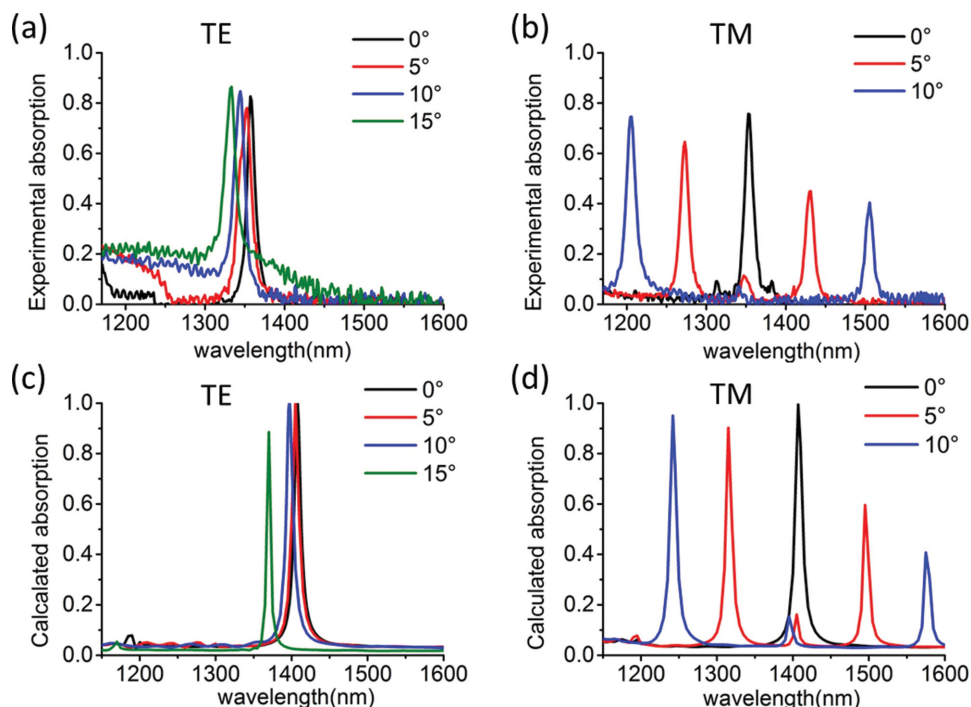
Figure 2. Measured spatially and spectrally resolved absorption of the PMMA absorber for a) TE ($E \perp S_{xz}$) at 0°, 5°, 10°, and 15° incident angles and b) TM ($H \perp S_{xz}$) at 0°, 5°, and 10° incident angles. Calculated results for c) TE mode ($E \perp S_{xz}$) and d) TM mode ($H \perp S_{xz}$) are presented.

Figure 3a,b shows the measured spatially and spectrally resolved absorption of the Au absorber, showing similar spatially and spectrally resolved absorption as that of the PMMA absorber. A nearly 70% peak absorption around 1436 nm with a bandwidth of 40 nm can be observed. The absorption peaks of TE and TM modes are also sensitive to the incident angle. For the TE mode, the absorption peak exhibits a blueshift from 1436 to 1404 nm as the incident angle increases from 0° to 15°, corresponding to a small wavelength-angle sensitivity of almost 2 nm per degree. For the TM mode, two absorption peaks can be observed. One largely redshifts while another largely blueshifts with the incident angle. Specifically, the two peaks are shifted to 1224 and 1623 nm at 10° incident angle, which corresponds to a large wavelength-angle sensitivity of nearly 20 nm per degree. Figure 3c,d shows corresponding calculated results of the Au absorber. For the Au absorber, the experimental bandwidth is larger than the PMMA absorber. Two factors contribute to the difference: (1) size and grain-boundary effects, which originate from the obvious grain in the gold surface, increase the loss of the gold film; and (2) large roughness in the edges of the Au nanodisks caused in the lift-off process leads to increased scattering loss.

Figure 4a,b shows the calculated spatially resolved absorption for the PMMA absorber at a fixed wavelength. Both TE and TM modes exhibit narrow spatially resolved absorption. For TE localized mode, the spatially resolved angular width at 1360 and 1380 nm wavelength is around 3.5°. For TM lattice mode at 1170 and 1285 nm wavelength, the spatially resolved angular width is around 0.75°, which is much narrower than the TE localized mode. The spatially narrow angular width is a signature of a large spatial coherence length at the corresponding

wavelength. The electric field of TE localized mode is predominately localized in comparison with the TM lattice mode, so the spatial coherence length of the TE localized mode is smaller than the TM lattice mode. As a result, the spatially extremely narrow angular width of TM lattice mode comes from the large spatial coherence. Here we define the absorption-angle sensitivity ($dA/(A \cdot d\theta)$) (absorption variation percentage $\Delta A/A$ divided by incident angle variation $\Delta \theta$) to characterize its spatial resolved ability in terms of the resonant absorbance. The absorption-angle sensitivity of the TE localized mode is around 26.6% per degree and that of the TM lattice mode around 77.5% per degree. For TM mode at wavelength 1170 nm, one localized mode appears at around 40° incident angle and its angular width is around 3.5°.

There are generally two methods to utilize this spatially and spectrally resolved narrowband absorber in spatial optical measurement. One way is to measure the spatially-resolved resonant peak wavelength by combining a light source and a spectrometer. This method is based on good linear relationship between absorption peak wavelength and incident angle θ at a large spectral range, and the aforementioned wavelength-angle sensitivity ($d\lambda/d\theta$) can be frequently used to characterize the measurement. This method features a relatively large measurement range (between −30° and 30°, shown in Figure S3b, Supporting Information) and a relatively low resolution by utilizing this spatially and spectrally resolved narrowband absorber. Considering a spectrometer with a spectral resolution of 0.02 nm, the resolution of angle measurement can be around 10^{-3} degree since the TM lattice mode exhibits a wavelength-angle sensitivity of nearly 15 nm per degree. The other way is to measure the spatial-resolved absorption at one fixed wavelength around
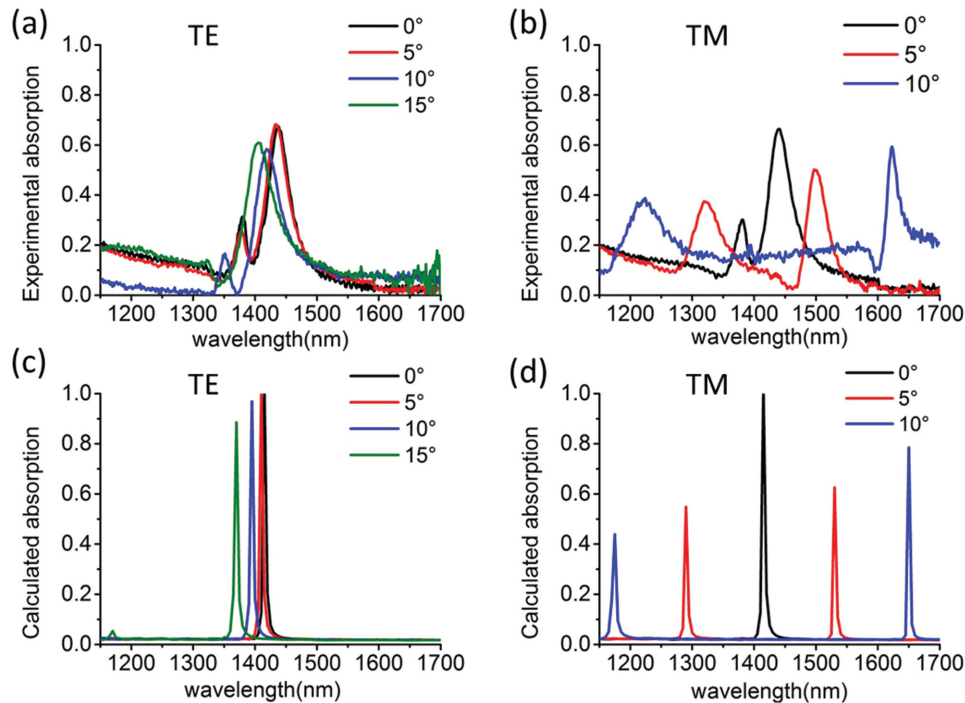
www.MaterialsViews.com

ADVANCED
OPTICAL
MATERIALS

www.advopticalmat.de

FULL PAPER

Figure 3. Measured spatially and spectrally resolved absorption of Au nanodisk array absorber for a) TE mode ($E \perp S_{xz}$) at 0°, 5°, 10°, and 15° incident angles and b) TM mode ($H \perp S_{xz}$) at 0°, 5°, and 10° incident angles. Calculated results for c) TE mode ($E \perp S_{xz}$) and d) TM mode ($H \perp S_{xz}$) are presented.
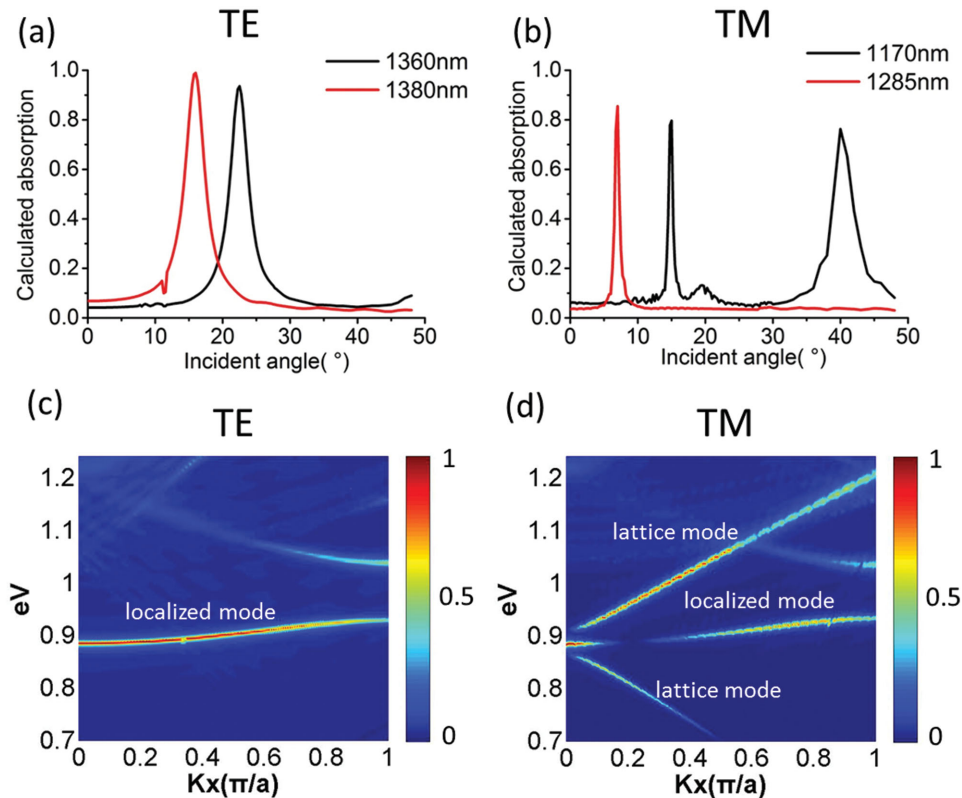

Figure 4. Calculated spatially-resolved absorption of the PMMA array absorber for a) TE mode ($E \perp S_{xz}$) at two fixed wavelengths (1360 and 1380 nm) and b) TM mode ($H \perp S_{xz}$) at two fixed wavelengths (1170 and 1285 nm). Calculated absorption spectra as functions of in-plane wave vector k_x (normalized to π/a) and photon energy (in eV) for c) TE and d) TM modes of the PMMA absorber. $k_x = (2\pi/\lambda)\sin\theta$.

the resonance by combining a light source and an optical power meter. This method exhibits a small measurement range (0.75° for TM lattice mode) due to the spatially-resolved narrowband absorption of this absorber. However, an extremely high angle resolution can be obtained. The aforementioned absorption-angle sensitivity ($dA/(A \cdot d\theta)$) (around 77.5% per degree for the TM lattice mode) can be used to characterize the measurement. Considering an optical power meter with a power resolution of 100 pW at an incident light power of 1 W (10^{-7} resolution), the resolution of angle measurement can be around 10^{-7} degree.

The spatially and spectrally resolved narrowband resonance can be explained in terms of the grating theory. The incident light cannot directly excite SPPs for a planar Au film because the wave vector of SPPs is always larger than that of the incident light. When Au film is coated with a 2D array, additional wave vector ($m2\pi/a$) is imposed resulting from periodicity of the 2D array. Assume that k_x is the in-plane wave vector of the incident light and a is the period of 2D array, the SPPs can be resonantly excited when their wave vectors satisfied the following equation

$$k_{SPP} = k_x \pm m\frac{2\pi}{a}, \ m = 0, \pm 1, \pm 2 \cdots \quad (1)$$

According to the grating theory, the limit of the angular width of resonant absorption is related to the number of the grating period N, the relative permittivity of the material, the grating period, and wavelength. In normal incidence case, the theoretical limit of the angular width at 1550 nm resonance for the Au absorber is 4.4 mrad at $N = 200$.

To further explore the origins of different spatially and spectrally resolved narrowband absorption between TE and TM modes, the SPP dispersion relations as well as field patterns for both the PMMA absorber and the Au absorber are calculated. We find that the Au absorber shows similar SPP dispersion relations and field patterns to those of the PMMA absorber; thereby, only the results for the PMMA absorber are presented. The calculated absorption spectra as functions of in-plane wave vector k_x and photon energy (in eV) for TE and TM modes are plotted in Figure 4c,d, respectively, which are also known as the SPP dispersion relations. For the TE mode, there is one strong absorption band with a small group velocity $d\omega/dk$ around 0.9 eV, which is a typical characteristic of a localized mode. For the TM mode, there are three strong bands around 0.9 eV: two bands with large group velocities are lattice modes and one band with a small group velocity is a localized mode. In the dispersion diagram, a large group velocity represents large angle sensitivity. For periodic structures, the photonics band gaps can be created in the vicinity of the Brillouin zone boundary owing to Bragg scatterings. As shown in the dispersion diagram for TM mode, the modes at band gap do not propagate at all, which can be regarded as standing waves with zero group velocity.

Absorption spectra as functions of wavelength and incident angle for TE and TM modes of the PMMA absorber are plotted in Figure S3a,b(Supporting Information). Both TE and TM localized modes are not sensitive to the incident angle.

However, the two TM lattice modes display a good linear relationship between the peak absorption wavelength and incident angle θ (15 nm per degree between −30° and 30°), which can be applied in spatial angle measurement.

The field patterns of resonant TE and TM modes of the PMMA absorber are shown in **Figure 5**. There are 5×5 unit cells in each field pattern. Since resonant TE modes (TM modes) have electric field E (magnetic field H) normal to incident plane S_{xz}, electric field E (magnetic field H) is thereby chosen in the field patterns. For the TE localized mode, the electric field (E_y) predominately concentrates in the PMMA regions. For the TM localized mode, the magnetic field (H_y) is strongly concentrated in both the PMMA regions and the air holes. For the two TM lattice modes, the fields alternate in phase in each unit cell along the direction of the wave vector k_x because of phase difference between adjacent unit cells. Wave fronts of the TM lattice modes are parallel to the y direction and propagate along x direction.

3. Conclusion

In summary, we experimentally demonstrate two kinds of spatially and spectrally resolved narrowband absorber, including the 2D PMMA nanohole array absorber and the 2D Au nanodisk array absorber. Their spatially and spectrally resolved absorption for both TE and TM modes is measured. The measured absorption bandwidth of PMMA absorber is 12 nm with a nearly 80% absorption, and the measured absorption bandwidth of Au absorber is 40 nm with a nearly 70% absorption. Both TE and TM modes support a localized mode with a small wavelength-angle sensitivity and absorption-angle sensitivity. Only TM mode supports a lattice mode with a large wavelength-angle sensitivity of nearly 15 nm per degree and a large absorption-angle sensitivity of 77.5% per degree. These spatially resolved narrowband absorbers have a potential application for spatial optical measurement, thermal emitter, optical filter, etc.

4. Experimental Section

Device Fabrication: The absorbers were fabricated as follows: for PMMA nanohole absorber, a 100-nm-thick Au film was deposited on glass substrate by sputtering. A 270-nm-thick PMMA (950K AR-P 672.03) was then spun onto the Au film as electron beam (E-beam) resisted and baked for 3 min. The PMMA was exposed to define the nanohole array by E-beam lithography and developed in 1:3 methyl isobutyl ketone/isopropyl alcohol (IPA) solution followed by rinsing in IPA. For gold nanodisk structure, the steps before development were the same. After development, a 50-nm-thick Au film was then deposited onto the sample by sputtering. The Au absorber was realized after liftoff by ultrasonic processing in acetone for 3 min.

Supporting Information

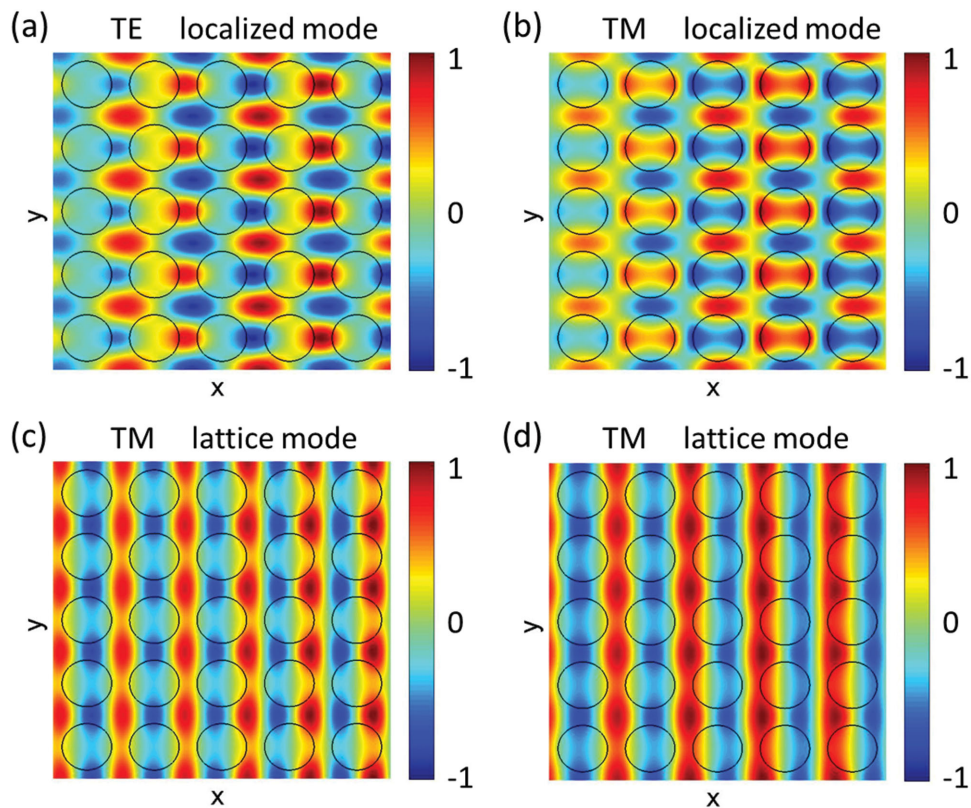Supporting Information is available from the Wiley Online Library or from the author.

www.MaterialsViews.com

ADVANCED
OPTICAL
MATERIALS
www.advopticalmat.de

FULL PAPER

Figure 5. The calculated resonant field patterns of 2D PMMA absorber. a) The electric field (E_y) of localized mode of TE polarization at 30° incident angle. b) The magnetic field (H_y) of localized mode of TM polarization at 30° incident angle. c,d) The magnetic field (H_y) of the two lattice modes of TM polarization at 5° incident angle. The patterns are taken at planes 135 nm above the Au films. The PMMA nanoholes are indicated by solid black outlines, and the color indicates the normalized amplitudes of E_y for TE mode and H_y for TM mode.

Acknowledgements

[1] M. K. Hedayati, F. Faupel, M. Elbahri, *Materials* **2014**, *7*, 1221.
[2] Y. Radi, C. R. Simovski, S. A. Tretyakov, *Phys. Rev. Appl.* **2015**, *3*, 037001.
[3] M. Pu, P. Chen, Y. Wang, Z. Zhao, C. Wang, C. Huang, C. Hu, X. Luo, *Opt. Express* **2013**, *21*, 11618.
[4] M. Pu, C. Hu, M. Wang, C. Huang, Z. Zhao, C. Wang, Q. Feng, X. Luo, *Opt. Express* **2011**, *19*, 17413.
[5] C. J. Chen, P. D. Lin, *Opt. Eng.* **2007**, *46*, 113604.
[6] C. Kuang, E. Hong, Q. Feng, *Opt. Eng.* **2007**, *46*, 051016.
[7] S. T. Lin, S. L. Yeh, C. W. Chang, *J. Opt. A: Pure Appl. Opt.* **2008**, *10*, 095304.
[8] H. G. Yun, S. H. Kim, H. S. Jeong, K. H. Kim, *Appl. Opt.* **2012**, *51*, 720.
[9] P. S. Huang, S. Kiyono, O. Kamada, *Appl. Opt.* **1992**, *31*, 6047.
[10] Y. Liu, C. Kuang, Y. Ku, *Opt. Laser Technol.* **2012**, *44*, 1346.
[11] M. Niraula, J. W. Yoon, R. Magnusson, *Opt. Express* **2015**, *23*, 023428.
[12] J. Hao, J. Wang, X. Liu, W. J. Padilla, L. Zhou, M. Qiu, *Appl. Phys. Lett.* **2010**, *96*, 251104.
[13] K. Aydin, V. E. Ferry, R. M. Briggs, H. A. Atwater, *Nat. Commun.* **2011**, *2*, 517.
[14] M. K. Hedayati, M. Javaherirahim, B. Mozooni, R. Abdelaziz, A. Tavassolizadeh, V. S. K. Chakravadhanula, V. Zaporojtchenko, T. Strunskus, F. Faupel, M. Elbahri, *Adv. Mater.* **2011**, *23*, 5410.
[15] C. M. Watts, X. Liu, W. J. Padilla, *Adv. Mater.* **2012**, *24*, OP98.
[16] A. Moreau, C. Ciracì, J. J. Mock, R. T. Hill, Q. Wang, B. J. Wiley, A. Chilkoti, D. R. Smith, *Nature* **2012**, *492*, 86.
[17] X. Chen, H. Gong, S. Dai, D. Zhao, Y. Yang, Q. Li, M. Qiu, *Opt. Lett.* **2013**, *38*, 2247.
[18] G. Tagliabue, C. Höller, H. Eghlidi, D. Poulikakos, *Nanoscale* **2014**, *6*, 10274.
[19] A. Tittl, A. U. Michel, M. Schäferling, X. Yin, B. Gholipour, L. Cui, M. Wuttig, T. Taubner, F. Neubrech, H. Giessen, *Adv. Mater.* **2015**, *27*, 4597.
[20] C. Hu, Z. Zhao, X. Chen, X. Luo, *Opt. Express* **2009**, *17*, 11039.
[21] N. Liu, M. Mesch, T. Weiss, M. Hentschel, H. Giessen, *Nano Lett.* **2010**, *10*, 2342.
[22] A. Tittl, M. G. Harats, R. Walter, X. Yin, M. Schäferling, N. Liu, R. Rapaport, H. Giessen, *ACS Nano* **2014**, *8*, 10885.
[23] S. Dai, D. Zhao, Q. Li, M. Qiu, *Opt. Express.* **2013**, *21*, 013125.
[24] K. Du, Q. Li, W. Zhang, Y. Yang, M. Qiu, *IEEE Photonics J.* **2015**, *10*, 1109.

FULL PAPER

[25] M. A. Kats, R. Blanchard, P. Genevet, F. Capasso, *Nat. Mater.* **2012**, *12*, 20.

[26] M. A. Kats, D. Sharma, J. Lin, P. Genevet, R. Blanchard, Z. Yang, M. M. Qazilbash, D. N. Basov, S. Ramanathan, F. Capasso, *Appl. Phys. Lett.* **2012**, *101*, 221101.

[27] M. Yan, *J. Opt.* **2013**, *15*, 025006.

[28] D. Zhao, L. Meng, H. Gong, X. Chen, Y. Chen, M. Yan, Q. Li, M. Qiu, *Appl. Phys. Lett.* **2014**, *104*, 221107.

[29] L. Meng, D. Zhao, Z. Ruan, Q. Li, Y. Yang, M. Qiu, *Opt. Lett.* **2014**, *39*, 1137.

[30] Z. Li, S. Butun, K. Aydin, *ACS Nano* **2014**, *8*, 8242.

[31] D. Xu, K. Zhang, M. Shao, H. Wu, R. Fan, R. Peng, M. Wang, *Opt. Express* **2014**, *22*, 25700.

[32] S. Ye, X. Zhang, L. Chang, T. Wang, Z. Li, J. Zhang, B. Yang, *Adv. Opt. Mater.* **2014**, *2*, 779.

[33] T. Søndergaard, S. M. Novikov, T. Holmgaard, R. L. Eriksen, J. Beermann, Z. Han, K. Pedersen, S. I. Bozhevolnyi, *Nat. Commun.* **2012**, *3*, 969.

[34] J. Beermann, R. L. Eriksen, T. Holmgaard, K. Pedersen, S. I. Bozhevolnyi, *Sci. Rep.* **2014**, *4*, 6904.

[35] J. Le Perchec, P. Quemerais, A. Barbara, T. Lopez-Rios, *Phys. Rev. Lett.* **2008**, *100*, 066408.

[36] A. Polyakov, K. F. Thompson, S. D. Dhuey, D. L. Olynick, S. Cabrini, P. J. Schuck, H. A. Padmore, *Sci. Rep.* **2012**, *2*, 933.

[37] P. A. Huidobro, X. Shen, J. Cuerda, E. Moreno, L. Martin-Moreno, F. J. Garcia-Vidal, T. J. Cui, J. B. Pendry, *Phys. Rev. X* **2014**, *4*, 021003.

[38] X. Shen, T. J. Cui, *Laser Photonics Rev.* **2014**, *8*, 137.

[39] J. J. Greffet, R. Carminati, K. Joulain, J. P. Mulet, S. Mainguy, Y. Chen, *Nature* **2002**, *416*, 61.

[40] V. M. Shalaev, W. Cai, U. K. Chettiar, H. K. Yuan, A. K. Sarychev, V. P. Drachev, A. V. Kildishev, *Opt. Lett.* **2005**, *30*, 3356.